The Thesis Committee for Ryan Gerald Andris
Certifies that this is the approved version of the following thesis:

The Effect of Restrictive Diffusion on Hydrate Growth

APPROVED BY
SUPERVISING COMMITTEE:

Supervisor:

Hugh Daigle

Kishore Mohanty

The Effect of Restrictive Diffusion on Hydrate Growth

by

Ryan Gerald Andris, B.S.

Thesis

Presented to the Faculty of the Graduate School of

The University of Texas at Austin

in Partial Fulfillment

of the Requirements

for the Degree of

Master of Science in Engineering

The University of Texas at Austin

May 2016

Dedication

To my family, friends, and teachers.

Acknowledgements

First and foremost, I want to thank my supervisor, Dr. Hugh Daigle, for his patience and guidance throughout my extensive learning process. I also want to thank Dr. Marc Hesse for teaching his elegant numerical solving method to any student willing to learn and Dr. Kishore Mohanty for donating his time to critique my work. In addition, thank you to my fellow methane hydrate researchers, Arash Shushtarian, Abhishek Bihani, and especially Michael Nole for freely exchanging ideas and offering some fresh eyes that made sure I never got so confident to think that I couldn't make mistakes.

I also want to thank The United States Department of Energy for supporting my research as well as Mr. S. Peyton Yates, Jr. and John and Kelli Weinzierl for sponsoring fellowships that went a long way towards funding my time spent at The University of Texas.

Lastly, I need to give a heartfelt thank you to my parents, Kathleen and Gerald Andris, for all of the sacrifices they have made that come with raising four children. I realize that I often made your lives difficult, but I know that I would not be here without you.

This work was supported by the Department of Energy under Award Number DE-FE0013919.

Abstract

The Effect of Restrictive Diffusion on Hydrate Growth

Ryan Gerald Andris, M.S.E.

The University of Texas at Austin, 2016

Supervisor: Hugh Daigle

Methane hydrate is formed naturally in a number of geologic settings around the world. The most predominant methane hydrate reservoirs are found in shallow oceanic basins at low temperatures and high pressures. A widely observed phenomenon in these oceanic sequences is extensive fine-grained sediments containing little to no hydrate interbedded with highly saturated sand bodies (20-60%). At Walker Ridge Block 313 in the Gulf of Mexico, one particular coarse-grained bed (approximately 3m-thick) is estimated to have methane hydrate occupying as much as 60% of the available pore space surrounded by hydrate-free clay. Here, I develop a numerical model that simulates methane hydrate growth in shallow oceanic basins in order to test whether diffusive transport of methane is a viable transport mechanism for forming highly saturated sand layers. I conclude that methane diffusion is likely responsible for the key identifying features of hydrate formation in interbedded sands and shales (i.e. greater hydrate saturations at the sand boundaries surrounded by hydrate-free zones in the fine-grained matrix). In addition, I show that the key parameters affecting the hydrate saturation profile include the amount of available methane for hydrate growth, thickness of the sand layer,

and the radius of the fine grained pore space. I also discuss the shortcomings of the developed model and what complexities need to be added to more accurately reproduce hydrate growth throughout intricate hydrogeologic systems.

Table of Contents

List of Tables

List of Figures

Chapter 1: Introduction

1.1 Natural Gas Hydrate as an Energy Resource

Natural gas hydrate, an ice-like structure composed of water and natural gas, can be found in large deposits in many regions throughout the world in a variety of geologic settings (Boswell & Collett, 2011). There have been a number of studies completed that have estimated the global inventory of this natural gas resource (Harvey & Huang, 1995; Arc, 2004; Klauda, & Sandler, 2005; Archer, Buffett, & Brovkin, 2009). Global supply estimates of methane hydrate have decreased over the years due to more conservative and sophisticated modeling approaches as well as a better understanding of the way hydrate is distributed in sediment, but it still has the potential to be a significant energy resource in the future. A recent report has estimated the volume of methane stored in natural gas hydrates to be between 3.3 and 3.6 x 10^{15} m^3 (Boswell et al., 2011).

Extensive fine-grained hydrate reservoirs found in shallow oceanic basins are the predominant source of methane for the above approximations. However; these reservoirs store natural gas hydrate at very low concentrations (i.e. saturations are generally found to be on the order of 1 to 3% and locally as high as 10%) (Boswell et al., 2011). In contrast, Boswell et al. (2011) estimates the total volume of gas in gas hydrate bearing sands to be on the order of 3 to 6 x 10^{14} m^3, a very small percentage of the total methane, but with concentrations in the range of 60% and projected potential recovery factors as high as 85% over the course of 30 years. Therefore, gas hydrate bearing sands have been identified as the most attractive target for industrial scale hydrate production. While sand reservoirs are the clear focus for those looking to extract methane from hydrates in the future, the transition from technically recoverable resources to economically recoverable resources will be challenging.

Figure 1.1: Evolution of Methane Hydrate as an Energy Resource through Time (Boswell et al., 2011)

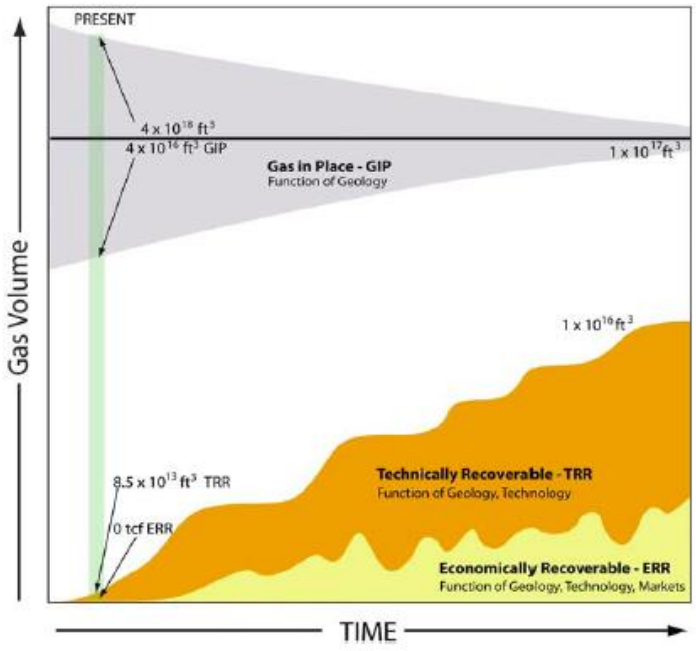

Figure 1.1 shows how the subdivisions of natural gas hydrate evolve as new technology develops and the global economic climate changes. The gas in place represents the estimated global supply which will become more constrained as additional studies are completed. The technically recoverable resources will increase as hydrate production technology matures. Economically recoverable resources, thought to predominantly consist of methane from gas hydrate bearing sands, should fluctuate in response to the change in global energy sources, government regulation policies, and to potential economically favorable extraction techniques.

1.2 Research Motivation

As natural gas hydrates in oceanic basins become a more viable source of energy production, a more complete understanding of what environmental conditions lead to massive hydrate deposits is needed. Massive hydrate deposits are defined as thick (i.e.

generally meters to potentially tens of meters) accumulations of methane hydrate at relatively high saturations. It is therefore important to gain further insight into what processes have the greatest impact on the distribution of hydrate saturations in a sediment matrix. One apparent process to study is the manner in which the methane necessary to form methane hydrate is transported into the potential hydrate reservoir. The migration mechanisms of methane are some of the least understood components of natural gas hydrate systems research, and it is the focus of this work.

1.3 Research Objectives

This report hypothesizes that the methane transport mechanism is the critical driver in determining the hydrate formation behavior in sand lithology. Specifically, the diffusive transport of biogenic, dissolved methane is studied in order to determine whether this process can produce sufficient methane flux into coarse-grained layers to produce massive hydrate deposits. To assess the behavior of methane diffusion, a one dimensional model is used to observe methane diffusion and hydrate formation on a sub-meter scale while putting constraints on available biogenic methane and methanogenesis rates. The model's hydrate system is based on the conditions found at Walk Ridge Block 313 in the northern Gulf of Mexico in order to compare results to the hydrate accumulation in this region. The key objectives of this work are to:

- Study the methane hydrate saturation profile generated in sand bodies with diffusion acting as the only methane transport mechanism;
- Examine the effect the diffusion coefficient of methane in sediment has on the formation of hydrate with diffusion acting as the sole methane transport mechanism;

- Observe how changing the amount of available biogenic carbon, and the rate at which it is converted to methane, changes the total saturation of the coarse-grained sediment;
- Compare the modeled results to the hydrate accumulation profile found at Walker Ridge.

The results of this research can be broadly applicable to a variety of hydrate systems. In addition, the hydrate saturation profile in the coarse-grained sediment should increase knowledge of what conditions lead to economically favorable hydrate reservoir targets. Understanding the ideal migration mechanisms and the amount of methane needed to produce these deposits can lead to more intelligent decisions regarding what regions to explore for hydrate production.

Chapter 2: Background

2.1 Introduction to Methane Hydrates

Natural gas hydrates are composed of a crystal lattice of water molecules that acts as a cage to enclose various low-molecular-weight gases such as methane, ethane, and carbon dioxide (Sloan & Koh, 2007). They are widely abundant in the upper few hundred meters of continental margin sediments where there are low temperatures, high pressures, and accessible methane sources (Kvenvolden, 1988; Buffett, 2000). The two dominant sources of natural gas are deep methane seeps and local biogenic methane production. The deeply sourced methane migrates upwards over long distances through the sediment column while biogenically produced methane is transported through the surrounding sediment over short distances. Biogenic methane production is generally restricted to fine-grained clays as they have much higher organic carbon content relative to coarse-grained sand.

Hydrates have already been discussed as a potential energy resource, but methane hydrates are also a potential concern for a significant climate change event due to the enormous volume of natural gas stored in these structures (Dickens et al., 1995; Archer, 2007). In addition, they are linked to submarine slope failure (McIver, 1982; Maslin et al. 2010). Obtaining a better understanding of the formation of natural gas hydrate and what effects their distribution within subsurface sediment should help assess the risk these substances pose to global climate events and their viability as an energy resource.

2.2 Hydrate Formation

The Gas Hydrate Stability Zone

Natural gas hydrates have the potential to be a significant energy resource in the future; however, hydrate reservoirs form much differently than conventional oil and gas

basins. The sediment that acts as a reservoir and seal for methane hydrates is defined by thermodynamics, a much different mechanism than the capillary pressure and buoyancy effects that produce traditional reservoirs (Clennell et al., 1999). Hydrates can be found in the gas hydrate stability zone (GHSZ), which is defined by the temperatures and pressures in which hydrate is thermodynamically stable (Figure 2.1).

Figure 2.1: An illustration of the GHSZ, BGHSZ, and the solubility of methane decreasing towards the seafloor (Tréhu et al., 2006)

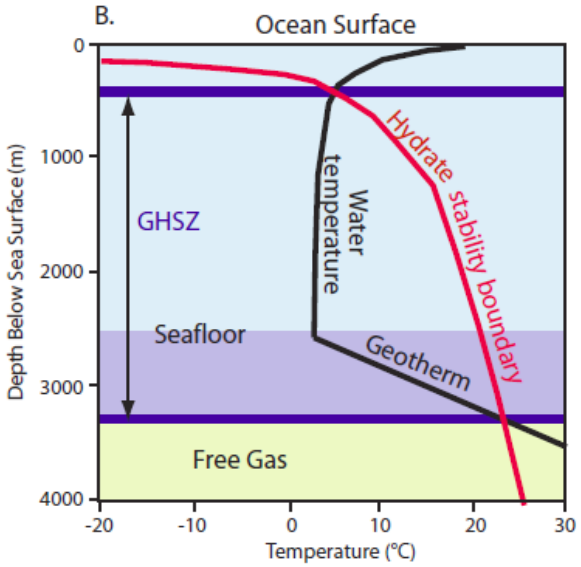

The pore fluid within the gas hydrate stability zone has a limit to the solubility of methane that increases with depth (Davie et al., 2004). If the concentration of methane exceeds the solubility limit, hydrate forms in the pore space. The depth at which the local pressure and temperature conditions of the oceanic basin coincide with the three phase equilibrium between water, methane hydrate, and natural gas marks the point at which hydrate will dissociate into free gas. This marked increase in low density fluid can often be seen in seismic measurements as a negative impedence contrast (Stoll et al., 1971). This

reflector is known as the bottom-simulating reflection (BSR) and it marks the base of the gas hydrate stability zone (BGHSZ).

Figure 2.2: A phase diagram illustrating the shift in stability conditions for methane hydrate in seawater due to an inhibition mechanism (Clennell et al., 1999).

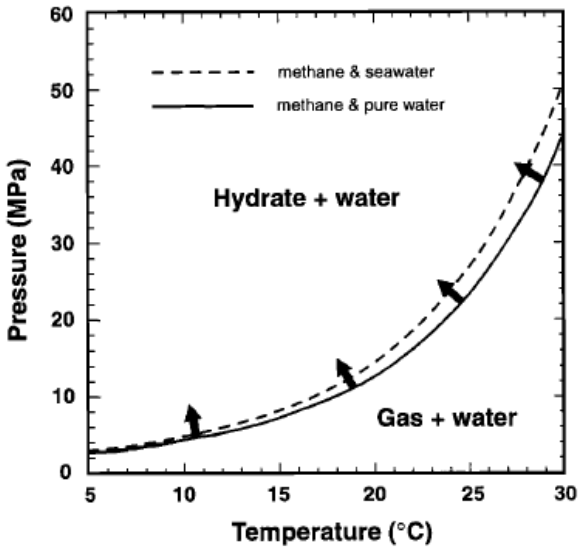

The depth of the BGHSZ is largely dependent on the geothermal gradient and is generally located at the pressure and temperature given by bulk phase equilibria (Hyndman & Davis, 1992; Davie et al., 2004). However, there are observed instances where the BGHSZ is located at a shallower depth than what would be expected based solely off pressure and temperature conditions (Westbrook et al., 1994; Paull et al., 1996). This phenomenon indicates that there is another component of hydrate stability acting as an inhibitor to hydrate growth (Figure 2.2). Such inhibitors can include dissolved salts or pore size effects (Clennell et al., 1999). In this work I focus on the pore size effects as these are believed to play an important role in localizing hydrate formation in sand layers when methane is supplied diffusively (e.g., Malinverno, 2010).

Pore Size Effects

As stated, this work focuses on hydrate growth inhibition in finer grained sediments due to capillary induced freezing point depression, otherwise known as the Gibbs-Thomson effect (Clennell et al., 1999; Daigle & Dugan, 2011). The freezing point in clay is depressed when compared to coarse-grained sand due to the presence of highly curved ice-water interfaces that increase the free energy of ice contained in small pores compared to larger pores (Everett, 1961). The ice contained in the small pores has an equivalently high curvature which magnifies the high surface energies at the ice water interface (Clennell et al., 1999). This thermodynamic effect is relatively absent in larger pores due to the increased ice radius. The effect is similar for hydrate nucleation since the formation of a solid hydrate phase out of liquid solution is analogous to freezing of ice. For this reason, an extra thermodynamic drive is required to induce hydrate formation from water and dissolved methane in fine-grained sediments. Therefore, lower temperatures, higher pressures, or a supersaturation of methane are needed to produce hydrate in oceanic muds compared to coarse-grained sands.

The model described in this paper focuses on the need for increased methane concentration to produce hydrate in clays (Figure 2.3). Figure 2.3 shows the difference in solubility between the fine-grained mud sediments and the coarse-grained sand. Also seen in this figure is the effect this difference in solubility concentration has on the distribution of methane throughout a sediment column. In general, sands do not have high organic matter content so an outside source of methane is needed to produce hydrate. The concentration gradient between the mud and sand causes the methane to move from areas of high concentration to areas of low concentration which produces hydrate in coarse-grained sediments.

Figure 2.3: Pore Water Methane Concentration Profile (Cook & Malinverno, 2013)

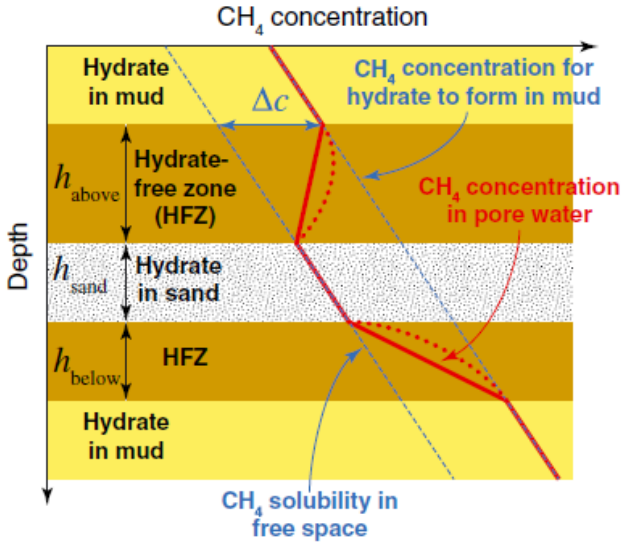

Methane Transport

There are two processes by which methane can enter a coarse grained layer and form hydrate. The first method of transportation is an advective flux which is effective over long distances (Boswell et al., 2012). The second transport mechanism, and the mechanism that will be the primary focus of this paper, is the diffusive flux of methane from organic-rich fine sediments to the coarse grained sand (Malinverno, 2010; Rempel, 2011). Diffusion is only an effective transportation mechanism over short migration distances.

2.3 Methane Diffusion in Bulk Sediment

As stated previously, the primary focus of this report is to analyze the effect methane diffusion has on hydrated growth in sand lithology. As hydrate is formed in the sand layers, it takes up pore space, thereby decreasing the fluid-filled pore volume. This decrease in fluid-filled pore volume affects the diffusion coefficient of methane in bulk sediment as shown in the following equations. First, the theoretical relationship between

the diffusion coefficient of methane in bulk sediment D_m and pore water D_o is as follows (Berner, 1980):

$$D_m = \frac{D_o}{\theta^2} \tag{1}$$

where θ^2 is equal to the tortuosity squared. Tortuosity is a geometric property of the porous medium that describes the total flow path of a substance as it avoids grain obstacles compared to the measured length of the porous medium (Peters, 2012). Therefore, tortuosity is inversely proportional to porosity and is a difficult property to measure directly. To combat this issue, Ullman and Aller (1982) showed the following relationship between tortuosity and the formation resistivity factor F:

$$\theta^2 = \phi F \tag{2}$$

where ϕ is the porosity of the porous medium. The formation resistivity factor can be put into terms of porosity by using the empirical relationship given by Archie (1942) as seen in equation (3).

$$F = \frac{1}{\phi^m} \tag{3}$$

The cementation exponent m has been found to have a range of values depending on the type of lithology. Archie (1942) found that m is in the range of 1.3-2 for sand and sandstones while Ullman and Aller (1982) found values between 2.5 and 5.4 are representative of clays. Equation (4) shows the final relationship between the diffusion coefficient of methane in pore water and bulk sediment related through the porosity of the porous medium.

$$D = \phi^{m-1} D_o \tag{4}$$

Again, the diffusion coefficient of methane in bulk sediment only changes if there is a change in porosity. Because porosity is restricted as hydrate forms, the new porosity can be found as a function of methane hydrate saturation h and initial porosity ϕ_o through equation (5).

$$\phi = (1 - h)\phi_o \tag{5}$$

2.4 Modeling Hydrate Formation

A Review of Previous Studies

There have been a number of models developed that describe the formation of hydrate within the natural gas hydrate stability zone (Rempel, 2011; Davie & Buffett, 2001, 2003; Malinverno, 2010). Rempel (2011) and Davie et al. (2001) focus on numerical solutions to solve methane mass balance equations relating to hydrate growth, and Malinverno (2010) derived simple analytic solutions to solve for the concentration of methane in pore fluid and the hydrate saturation in pore space.

Malinverno (2010) uses a steady state model to examine how varying pore geometry between sedimentary layers can cause diffusive transport of methane. The methane diffuses from areas of high pore water concentration to areas of low concentration which leads to hydrate growth in coarse-grained sands embedded in more finely grained background material. The analytical solutions focus on the key drivers in hydrate formation, and they are able to determine that diffusion is a plausible method for transporting methane from fine-grained sediments to isolated sand layers. Malinverno (2010) also concludes that microbial methanogenesis can produce enough methane to account for hydrate saturations seen in various reservoirs throughout the world. Both

findings help to create a solid foundation for the model described in this report and validate key assumptions described in Chapter 3.

The numerical model presented by Davie and Buffett (2001) also assumes methane is added through sedimentation and microbial methanogenesis, but the analysis is limited to homogeneous bulk sediment. A key motivation in their research is to gain a better understanding of how the methane supply is regulated. They present a simple model for the rate of methanogenesis that is limited by the total amount of organic carbon available at the seafloor. The initial organic carbon value, given as a weight percentage of the sediment, decreases as the organic matter is buried in the sediment column due to methanogenesis. However, Malinverno (2010) argues that the ratio of the molar mass between methane and carbon used here is too low, and it may underestimate maximum hydrate saturations. In addition, Davie et al. (2001) uses a one-step conversion to get from methane to hydrate, an assumption that will also be adopted here. The proposed model for microbial methane production and formation of hydrate will be discussed further in the following sections.

Rempel (2011) modeled the effect discontinuous sediment properties have on hydrate formation on continental margins, and showed that hydrate preferentially forms in coarse-grained sediments when bounded by fine-grained clay. However, Rempel (2011) utilizes both advective and diffusive transport of methane and did not specifically analyze the diffusion coefficient of natural gas or account for sedimentation. In addition, the methane transport mechanisms are not treated as a function of saturation. The goal of this study is to expand upon the above publications and to focus specifically on the diffusive transport of methane and its effect on the hydrate distribution in a coarse-grained sand as it moves through the sediment column.

Rate of Microbial Methane Generation

Starting at the top of the sediment column, the rate of methanogenesis from the seafloor to the base of the sulfate reduction zone (BSRZ) is very low (Reeburgh, 2007) and is approximated as zero in this study. The sulfate reduction zone is dominated by microbes whose primary respiration process is the reduction of sulfate which inhibits any microbial methane production (Claypool & Kaplan, 1974; Martens & Berner, 1974; Reeburgh, 2007). In addition, some organic matter is lost at the base of the sulfate reduction zone due to anaerobic oxidation (Reeburgh, 2007).

Once past the BSRZ, the organic carbon in the clay, represented as a dry weight percentage α, will diffuse out of the sediment and increase the methane concentration in the pore water. Davie et al. (2001) models this process as a single step with the conversion factor k_α. A key component of k_α is the ratio of the molar mass between methane and carbon. This ratio controls the limit of organic matter that can be converted to methane. Malinverno (2010) makes the argument for using a 16/12 ratio, which is the ratio of the molar masses of methane and carbon. He contends that studies that use a ratio of 16/30, which is the ratio of the molar masses of methane and formaldehyde, which is often used as a generic organic molecule (Davie et al. 2001, 2003), underestimate the microbial methane production. This work will adopt the methane-carbon molar mass ratio used by Malinverno (2010). The complete model employed is shown with equation (6) where ρ_g is the grain density and ϕ is the porosity.

$$\frac{16}{12}\rho_g \frac{1-\phi}{\phi}\alpha = k_\alpha \alpha \tag{6}$$

The rate at which methanogenesis occurs will steadily decrease with depth as the amount of available organic carbon α decreases from its initial value α_{BSRZ} at the base of

the sulfate reduction zone. Davie et al. (2001) modeled the local mass balance for α as seen in the following equation:

$$\frac{\partial \alpha}{\partial t} = -\lambda\alpha - v_s \frac{\partial \alpha}{\partial z} \tag{7}$$

where λ is the reaction rate constant of methanogenesis and v_s is the sedimentation rate. The rate of microbial methane generation is determined by multiplying the reaction rate constant by the mass of methane determined using equation (6). This method will be discussed further in Chapter 3.

Rate of Hydrate Accumulation

An assortment of studies have generated predictions for rates of hydrate accumulations in sediment (Davie et al. 2001, 2003; Rempel & Buffett, 1997). A straightforward model for hydrate growth, and the one utilized here, assumes that hydrate forms slowly enough so that the latent heat produced from the liquid water phase changing to a solid phase is small enough that the temperature profile within the GHSZ is constant. In addition, because the rate of hydrate formation is low, the local methane concentration within the hydrate stability zone will approach the local equilibrium value (see Davie et al., 2004).

2.5 Walker Ridge, Gulf of Mexico

Since 2005 the Gulf of Mexico has been rigorously studied with respect to its potential as a methane hydrate reservoir (Boswell et al. 2011). The Bureau of Ocean Energy Management estimated that sand reservoirs in this region contain approximately 200 million cubic meters of gas-in-place which accounts for about of a third of the total estimated volume. The high concentrations of natural gas hydrate observed in coarse-grained sands marks this area as an ideal comparison for the model developed in this study.

Figure 2.4: A map of the deepwater Gulf of Mexico featuring gas hydrate related research expeditions. This work focuses on the conditions found in Hole H drilled at Walker Ridge Block 313 (Cook et al., 2013)

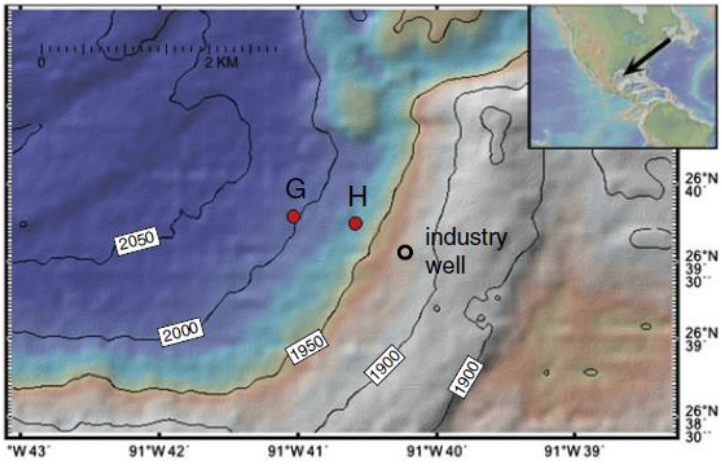

Specifically, Walker Ridge Block 313 is well suited for the one dimensional model of hydrate growth presented in this report. During the second leg of the DOE-Chevron Joint Industry Project (JIP) two holes were drilled in this locality (Figure 2.4). Both of these wells showed interbedded muds and thin gas-hydrate-bearing sands with varying degrees of hydrate saturation (Boswell et al. 2011). An unexpected finding of these research expeditions is relatively shallow occurrences of hydrate bearing sands far removed from sources of free gas. The hydrate here is likely sourced by local methanogenesis in fine-grained clays where the methane produced diffuses into the sand through short migration pathways. A type example of this phenomenon is the Unit A sand in Walker Ridge Block 313 Hole H shown in Figure 2.5 at ~290 mbsf. This sand unit is bounded by fairly thick fine-grained sediments that generally contain relatively high amounts of organic carbon. The proposed mechanism of hydrate formation by Cook et al. (2013), and the process tested in the model developed in this study, is the short migration of methane from clay to sand. The hydrate-free zone (HFZ) seen bordering the boundaries of the Unit

A sand could be a key characteristic of this method of hydrate formation and is a potential outcome of the model discussed in detail in Chapter 3.

Figure 2.5: Well logs and interpretation of the region surrounding a hydrate filled coarse-grained sand layer at Walker Ridge Hole 313-H (Cook et al. 2013)

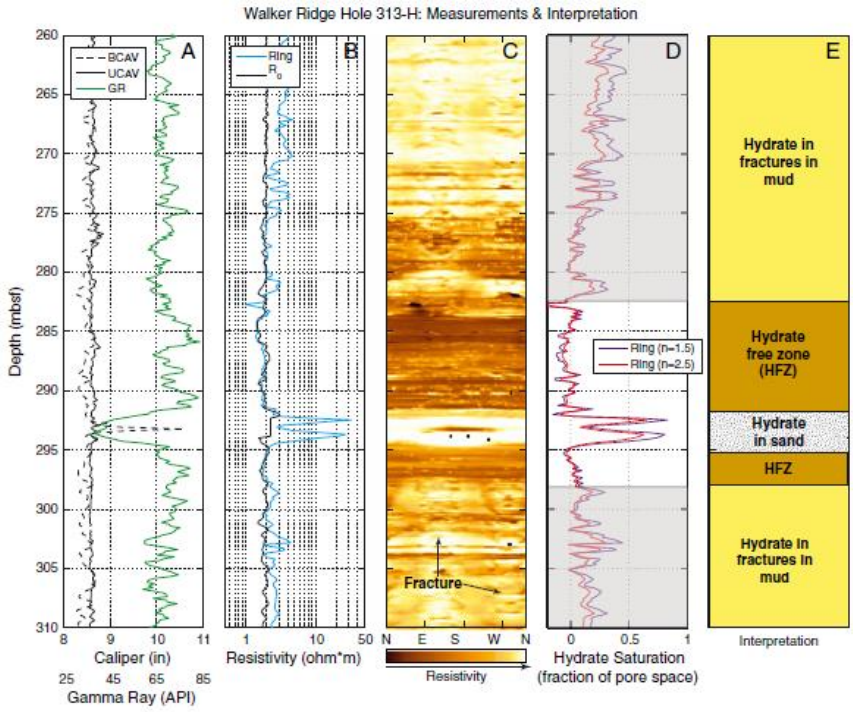

Chapter 3: Methods

3.1 Key Modeling Assumptions

Figure 3.1: Unit volume of sediment (Malinverno, 2010).

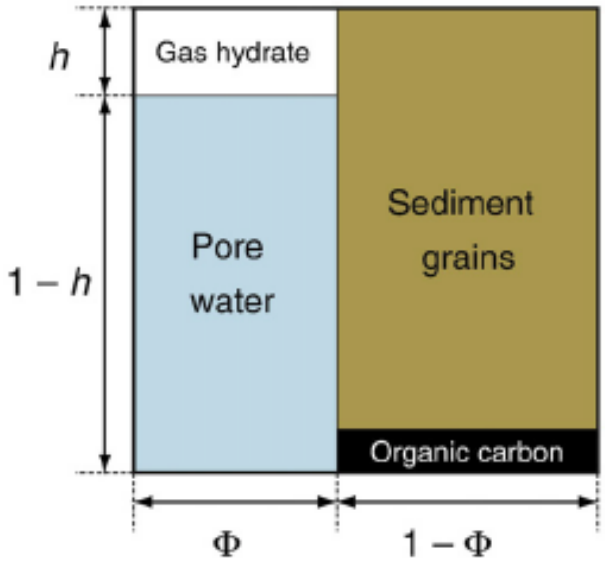

Gas hydrate growth can be quantitatively modeled by balancing the mass of methane produced and transported throughout the hydrate stability zone. The model developed here is one-dimensional, and Figure 3.1 shows the unit volume of sediment at a single moment in time. The only phases present in the pore space are water and hydrate. This effect occurs because the mass balance model assumes local thermodynamic equilibrium, and therefore, gas cannot exist as a free phase in the GHSZ with excess amounts of water present (Zatsepina et al., 1998). If gas were to evolve, it quickly combines with water to form hydrate (Sloan et al., 2007).

Additionally, the only source of methane is microbial methanogensis, an anaerobic respiration process. Microbes reduce complex organic molecules to small hydrocarbon chains (e.g. methane) that then dissolve into the pore fluid. Hydrate forms when the dissolved methane reaches the limit of solubility. This model is assumed to be situated

away from methane vents in order to focus exclusively on the diffusive transport of methane. Supplemental assumptions will be discussed in the appropriate section within this chapter.

3.2 Mass Balance of Methane

Following the initial approach laid out by Malinverno (2010), the mass balance of methane at a depth z below the seafloor can be expressed through two coupled equations. The first equation is concerned with the concentration of methane c in the pore fluid:

$$\frac{\partial}{\partial t}[\phi_o(1-h)c] = \frac{\partial}{\partial z}\left[D\phi_o(1-h)\frac{\partial c}{\partial z}\right] - \frac{\partial}{\partial z}\left[v_f\phi_o(1-h)c\right] - c_h q_h + f_s \quad (8)$$

while the second mass balance equation models the mass fraction of hydrate h:

$$\frac{\partial}{\partial t}[\phi_o h] = -\frac{\partial}{\partial z}[v_s\phi_o h] + q_h \quad (9)$$

where ϕ_o is equal to the initial porosity, D is the diffusion coefficient of methane in sediment, v_f is the pore fluid velocity, v_s is the sedimentation rate, c_h is the concentration of methane in hydrate, q_h is the rate of formation of gas hydrate, and f_s is the methane source term. A summary of these variables, and variables in subsequent equations, and their units can be found in Table 3.1.

Table 3.1: Notation and Modeling Variables [a] from Malinverno (2010); [b] from Cook et al. (2013); [c] from Sloan (2007); [d] from Davie et al. (2004); [e] from Boswell et al. (2012); [f] from Henrey et al. (1999); [g] from Milkov and Sassen (2001); [h] from Kastner, Claypool, and Robertson (2008).

Symbol	Definition	Value	Units
c	Methane concentration in pore water		kg m^{-3}
c_h	Methane concentration in gas hydrate[a]	119.3	kg m^{-3}
D	Diffusion coefficient of methane in sediment		m^2 s^{-1}
D_o	Diffusion coefficient of methane in pore water	$8.212e^{-10}$	m^2 s^{-1}

Table 3.1, cont.

f_s	Rate of microbial methane production		kg m^{-3} s^{-1}
h	Hydrate saturation		
k_α	Conversion factor from α to methane		kg m^{-3}
m	Archie's cementation exponent[b]	1.9	
n	Molar ratio of methane to water in hydrate[c]	5.75	
q	Fluid flux		m s^{-1}
R	Gas Constant	8.314	m^3 Pa K^{-1} mol^{-1}
r_{sh}	Pore radius of fine-grained material	$50e^{-9}$	m
s_{BGHSZ}	Methane solubility at BGHSZ[d]	2.68	kg m^{-3}
s_{sh}	Methane solubility in fine-grained pore water		kg m^{-3}
s_{ss}	Methane solubility in coarse-grained pore water		kg m^{-3}
T_G	Temperature gradient[g]	.018	°C m^{-1}
T_{SF}	Temperature at the seafloor[e]	276	K
T_*	Characteristic temperature for calculation s_{ss}[d]	14.4	°C
V_b	Molar volume of water in hydrate	$2.26e^{-5}$	m^3 mol^{-1}
v_f	Velocity of pore fluid	$-2.14e^{-11}$	m s^{-1}
v_s	Sedimentation Rate[b]	$2.14e^{-11}$	m s^{-1}
z_{BGHSZ}	Depth to BGHSZ[e]	900	m
z_{BSRZ}	Depth to base of sulfate reduction zone[h]	9	m
α	Metabolizable organic carbon		Dry weight %
α_{BSRZ}	Available metabolizable organic carbon at BSRZ		Dry weight %
γ	Hydrate - pore water interfacial tension[f]	.027	N m^{-1}
θ	Tortuosity		
ϕ	Sediment column porosity		
ϕ_o	Original sediment column porosity[b]	.35	
λ	Reaction rate constant of methanogenesis		s^{-1}
ρ_g	Density of sediment grains	2750	kg m^{-3}

An additional assumption is that the hydrate-free porosity is constant throughout the sediment column. Ignoring compaction introduces some error that is predominantly confined to the shallower sections of the basin, and it should not interfere significantly with modeling results. However, porosity is a function of hydrate saturation. The model

developed here accounts for hydrate saturation explicitly so that the porosity is updated at every time-step according to the following equation:

$$\phi = (1 - h)\phi_o \tag{10}$$

Accounting for equation (10) and subsequently combining equations (8) and (9) leaves:

$$\frac{\partial}{\partial t}[\phi c] = \frac{\partial}{\partial z}\left[D\phi \frac{\partial c}{\partial z}\right] - \frac{\partial}{\partial z}\left[v_f \phi c\right] - \frac{\partial}{\partial t}[\phi h c_h] - \frac{\partial}{\partial z}[v_s \phi h c_h] + f_s \tag{11}$$

The term $\frac{\partial}{\partial z}[v_s \phi h c_h]$ represents the methane trapped in hydrate moving down at the rate of sedimentation. This behavior is also handled explicitly and does not appear in the partial differential equation leaving:

$$\frac{\partial}{\partial t}[\phi c + \phi h c_h] = \frac{\partial}{\partial z}\left[D\phi \frac{\partial c}{\partial z} - v_f \phi c\right] + f_s \tag{12}$$

In addition, the simulation assumes the solution to the mass balance equation is the concentration of methane in pore water. The methane that exceeds the solubility limit is separated explicitly, which further simplifies the PDE to:

$$\frac{\partial}{\partial t}[\phi c] = \frac{\partial}{\partial z}\left[D\phi \frac{\partial c}{\partial z} - v_f \phi c\right] + f_s \tag{13}$$

Fluid Velocity

Due to the absence of advection, the interstitial fluid velocity is equal and opposite to the rate of sedimentation v_s. The fluid velocity v_f can be calculated using equation (14) where ϕ is equal to porosity. The solution to equation (14) is equivalent to the fluid flux q shown in equation (15).

$$v_f = -v_s * \phi \tag{14}$$

$$q = v_f \tag{15}$$

Realistically, a decrease in pore space would reduce the rate of fluid flow within the sediment column, but this one-dimensional model assume a constant fluid velocity. The mass balance is now reduced to:

$$\frac{\partial}{\partial t}[\phi c] = \frac{\partial}{\partial z}\left[D\phi\frac{\partial c}{\partial z} - qc\right] + f_s \tag{16}$$

Diffusion Coefficient of Methane

Using the equation derived in Chapter 2.3, the diffusion coefficient of methane in sediment *D* can be calculated using equation (17). This equation only applies when looking to see the effect a changing diffusion coefficient has on the distribution of hydrate in a coarse-grained layer. Otherwise, the equation needs only be used once when ϕ is equal to ϕ_o to obtain a constant diffusion coefficient employed at all times.

$$D = \phi^{m-1}D_o \tag{17}$$

Microbial Methane Generation

As discussed in Chapter 2.4 the conversion from organic carbon to dissolved methane in pore water is a one step process that utilizes a conversion factor k_α that is equivalent to:

$$k_\alpha = \frac{16}{12}\rho_g\frac{1-\phi}{\phi} \tag{18}$$

where ρ_g is the sediment grain density and 16/12 is the molar ratio between methane and carbon. Because k_α is dependent upon porosity, it must be updated in time as the hydrate saturation changes. This term is then used in the steady state solution of equation (7) for the rate of microbial methane generation shown in equation (19) (Malinverno, 2010). One key point to emphasize is that f_s is equal to zero in sand layers due to low organic content.

$$f_s(z) = k_\alpha \lambda \alpha_{BSRZ} exp\left[-\frac{\lambda}{\omega}(z - z_{BSRZ})\right] \quad (19)$$

The model sensitivities were tested by varying the two variables used to determine the rate of methanogenesis, the initial amount of metabolizable carbon α_{BSRZ} and the reaction rate constant λ. Values for α_{BSRZ} were taken from Malinverno (2010), and while the reaction rate is less understood (Davie et al., 2001), it has been found to be on the order of 10^{-13} s^{-1} (Davie et al., 2003).

3.3 Solubility of Methane

Sand Lithology

The methane solubility behavior in pore water is clearly defined in Davie et al. (2004), and it is explicitly calculated using equation (20). As previously stated, s_{ss} is the solubility of methane in sandstone, s_{BGHSZ} is the solubility of methane at the BGHSZ, T_G is the geothermal temperature gradient, z describes a depth below the seafloor, and T_* is a characteristic temperature further expanded upon in Davie et al. (2004) along with the procedure for calculating the solubility of methane at the base of the gas hydrate stability zone. Methane solubility below the base of gas hydrate stability can be approximated as s_{BGHSZ} (Davie et al., 2004).

$$s_{ss} = s_{BGHSZ} exp\left(\frac{T_G}{T_*}(z - z_{BGHSZ})\right) \quad (20)$$

Clay Lithology

The solubility of methane in fine-grained sediment s_{ss} is increased relative to that of sandstone due to the effects described in Chapter 2.2. Clennell et al. (1999) derives an analytic expression for the methane solubility in shale as a function of the sandstone solubility.

$$s_{sh} = \left(exp\left(\frac{2\gamma}{r_{sh}}\right) \frac{n\bar{V}_b}{R(T_{SF} + \theta z)} \right) s_{ss} \quad (21)$$

Here, γ is the interfacial tension between the pore water and solid hydrate, r_{sh} is the average pore radius of the fine-grained sediment, n is the molar ration of methane to water in hydrate, V_b is the molar volume of water in hydate, R is the gas constant, and T_{SF} is the temperature at the seafloor.

3.4 SOLUTION METHOD

The mass balance defined above is solved numerically in one dimension using an implicit finite difference model. The methane concentration in pore water is solved at every time step and then compared to the solubility of methane at every depth. Any methane in excess of solubility at a certain depth is then subtracted from the total amount of methane to form hydrate. This process is described in equation (22) where c_h is the concentration of methane in hydrate. The methane trapped in the hydrate is subsequently moved down at the sedimentation rate independent of the pore fluid. Conversely, if hydrate is present while c is less than s_{ss} or s_{sh} then the hydrate will partially or fully dissociate to increase the concentration of methane in pore fluid.

$$h = \frac{c/c_h}{1 + c/c_h} \quad (22)$$

Initial Conditions

As discussed in Chapter 2, hydrate accumulates slowly on geologic timescales, which allows the concentration of methane to reach its solubility point. Here, the model assumes that the concentration of methane has reached steady state values throughout the sediment column at the start of the simulation. This supposition means that the zone in which hydrate will form is defined prior to formation of any hydrate.

Boundary Conditions

This model employs Dirichlet Boundary Conditions. The concentration of methane in the first grid block is set to zero because it corresponds to the base of the sulfate reduction zone. The base of the model assumes a concentration gradient of zero as the rate of microbial methane production approaches zero. Therefore; the methane concentration of the final grid block is equal to the grid block above it.

Additional Notes

Prior to introducing a coarse-grained sand layer, I first let the hydrate saturation profile in the fine-grained sediments reach steady state.

Chapter 4: Results and Discussion

4.1 Results

As stated, before introducing the coarse-grained sand layer, I allowed the hydrate saturation in the fine-grained clays reach steady state values as shown in Figure 4.1. The layer of sand, at approximately the same thickness as the sand found at Walker Ridge Block 313 Hole H (i.e. ~3m), was then introduced at the base of the sulfate reduction zone, 9 meters below the seafloor, as observed in the Keathley Canyon region of the Gulf of Mexico (Kastner et al., 2008). Subsequently, the sand bed reached its limit of methane solubility shown in Figure 4.2. Once the sand was in the hydrate stability zone methane began to diffuse into the coarse-grained layer due to the concentration gradient between the clay and sand lithology (Figure 4.3).

Figure 4.1: Hydrate Saturation in fine-grained clays at steady-state values.

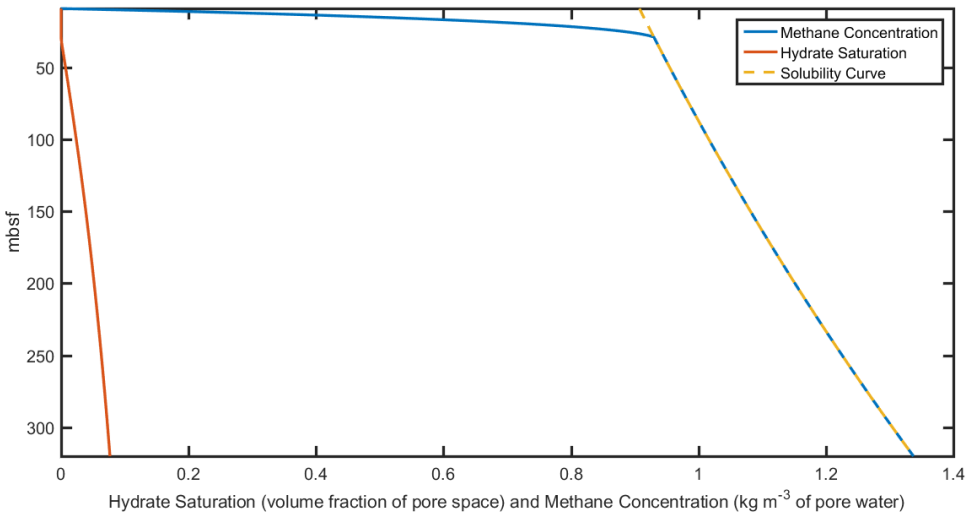

Depending on the parameters defined at the start of the simulation, a different hydrate saturation profile developed as the sand moved through the sediment column. The key variables analyzed here included the available metabolizable organic carbon at the

BSRZ α_{BSRZ}, the reaction rate constant of methanogenesis λ, and the difference between a constant diffusion coefficient of methane in sediment D_m and a changing diffusion coefficient as a function of porosity. In addition, I briefly looked at how the thickness of the sand and the radius of the clay pores affected hydrate growth.

Figure 4.2: Sandstone layer reaching the limit of methane solubility.

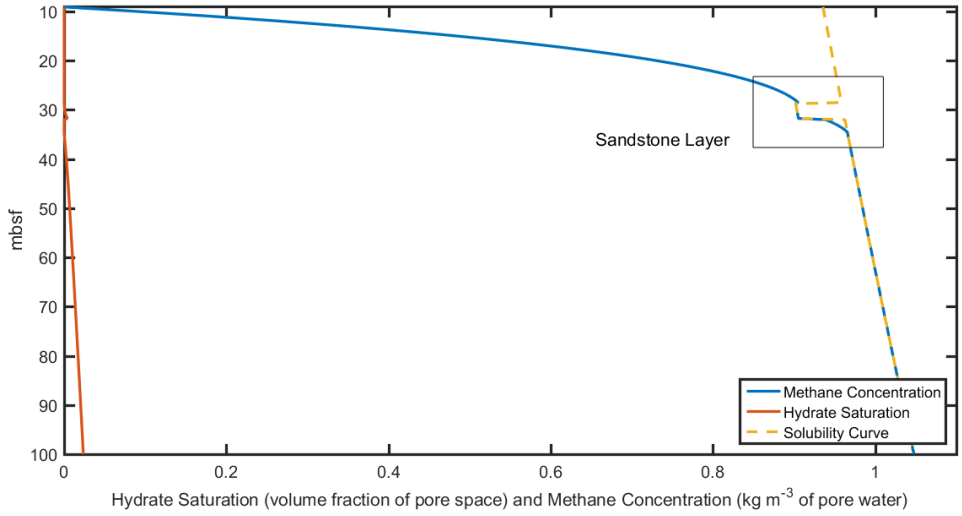

Figure 4.3: Hydrate saturation profile in sand starting to develop.

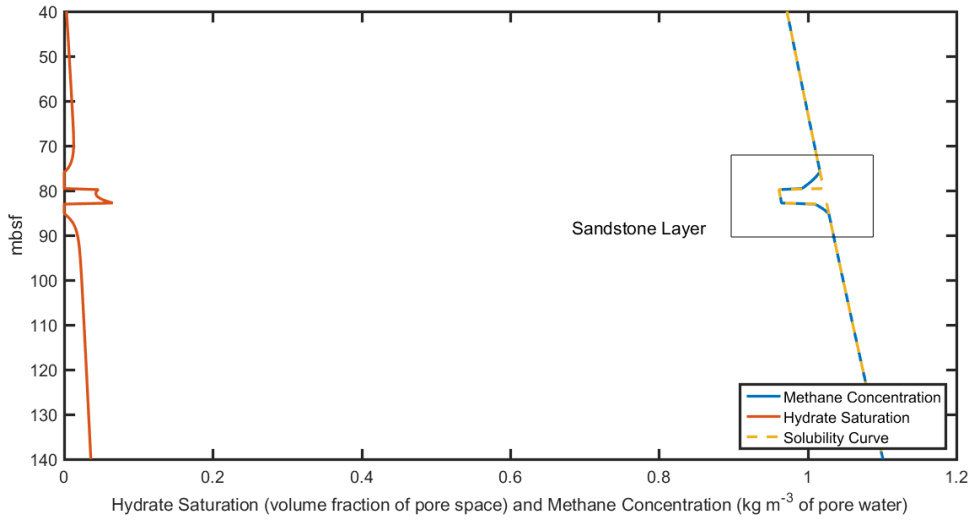

Changing α_{BSRZ}

The first parameter studied was the amount of available metabolizable organic carbon at the BSRZ. While changing α_{BSRZ}, λ was held constant at $0.2 \cdot 10^{-13}$ s^{-1}, the clay particle radius was equal to 50 nm, and the diffusion coefficient of methane was always calculated as a function of porosity which changed as hydrate grew in the pore space. Figures 4.4 was generated with α_{BSRZ} values of 0.10%, 0.12%, and .20%.

Figure 4.4: Changing α_{BSRZ}

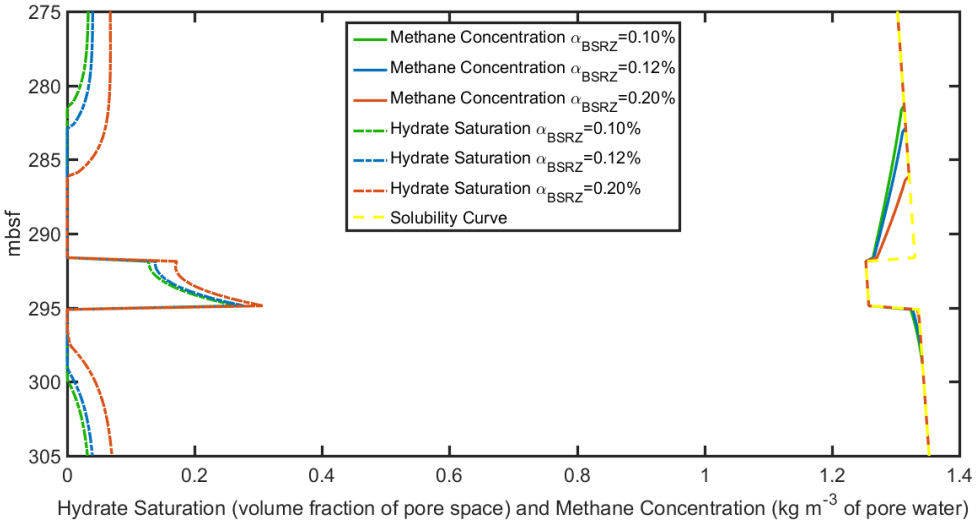

Table 4.1: α_{BSRZ} Analysis; * indicates values found in Hole H at Walker Ridge Block 313

α_{BSRZ} (weight %)	HFZ above sand (m)	HFZ below sand (m)	*h* at upper sand boundary	*h* at lower sand boundary	min *h* in sand	mass CH_4 in sand (kg)
	10.3*	3.20*	.6*	.6*	.15*	
0.10	10.5	4.25	.127	.266	.127	82.15
0.12	9.00	3.25	.138	.277	.138	87.65
0.20	5.75	1.00	.172	.307	.170	105.2

Table 4.1 gives an overview of the results obtained from the three simulations. As expected, increasing the available organic carbon increased the hydrate saturations in the coarse-grained sand. However, the values do not approach the saturations observed at Walker Ridge. The simulation that most closely reproduced the magnitude of the hydrate free zones above and below the sand also produced hydrate saturations merely one-third of those seen in the Gulf of Mexico. It is also worth noting that the trend between organic carbon content and the mass of methane in sand is non-linear. Increasing α_{BSRZ} by 20% caused a 6.7% increase in mass of methane while a 100% increase in carbon produced a 28% increase in mass of methane. Similarly, doubling the amount of methane only increased the hydrate saturation at the lower and upper sand boundaries by 15% and 35%, respectively.

Changing λ

To focus solely on the change in the rate constant of methanogenesis, α_{BSRZ} was held at .1%, the clay pore radius at 50nm, and the diffusion coefficient of methane in sediment was calculated as a function of porosity. Figures 4.5 shows the simulation results for λ values of $0.2 \cdot 10^{-13}$ s^{-1}, $0.5 \cdot 10^{-13}$ s^{-1}, $1.0 \cdot 10^{-13}$ s^{-1}, and $2.0 \cdot 10^{-13}$ s^{-1}.

The overall trend of data (Table 4.2) is similar to that of changing the available organic carbon content. An increase in the rate of constant of methanogenesis showed a marked decrease in the magnitude of hydrate free zones, an increase in overall saturation, and therefore, an increase in total mass of methane. Again, resultant hydrate saturations did not approach those seen in Hole H. Additionally, the trend between λ and mass of methane is also non-linear. A 900% increase in λ only created a 63% increase in mass of methane.

In contrast, it does appear that increasing λ produces a more significant rind in the sand, seen clearly in the Hole H logs in Figure 2.5, when compared to increasing α_{BSRZ}. The differences between the minimum hydrate saturation and maximum hydrate saturation (at the upper sand boundary) here are significantly greater than the previously discussed simulations.

Figure 4.5: Changing λ

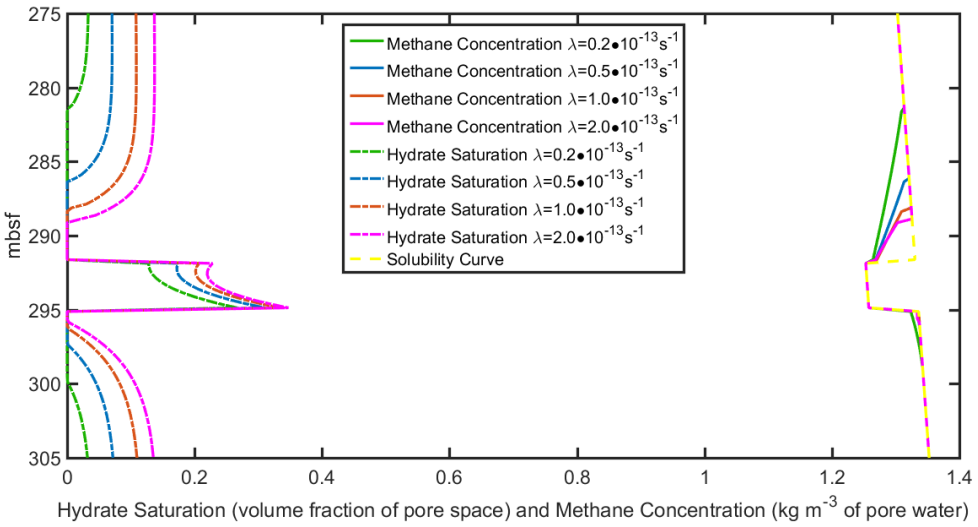

Table 4.2: λ Analysis; * indicates values found in Hole H at Walker Ridge Block 313

λ (s^{-1})	HFZ above (m)	HFZ below (m)	*h* at upper sand boundary	*h* at lower sand boundary	min *h* in sand	mass CH_4 in sand (kg)
	10.3*	3.20*	.6*	.6*	.15*	
$0.2 \cdot 10^{-13}$	10.5	4.25	.127	.266	.127	82.15
$0.5 \cdot 10^{-13}$	5.75	1.75	.174	.310	.172	106.7
$1.0 \cdot 10^{-13}$	3.75	1.50	.207	.335	.201	123.6
$2.0 \cdot 10^{-13}$	3.00	1.00	.228	.347	.220	134.1

Changing D_m

To investigate the effect changing the diffusion coefficient of methane in sediment has on simulated results, previous simulations were run a second time with the only difference being a constant diffusion coefficient. New hydrate saturation profiles are compared to their variable diffusion coefficient counterparts in Figures 4.6 and 4.7.

Figure 4.6: $\alpha_{BSRZ} = 0.10\%$; $\lambda = 2.0 \cdot 10^{-13}$ s^{-1}; $D_m = 3.9 \cdot 10^{-10}$ m^2 s^{-1} (Cook et al., 2013)

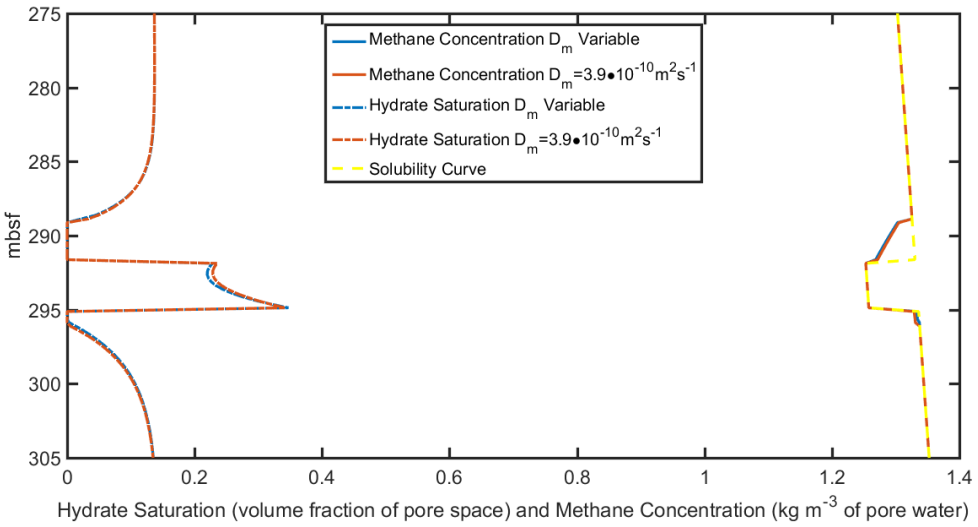

A constant diffusion coefficient of methane slightly increased the magnitude of the hydrate free zone below the sand layer, produced a more homogeneous hydrate saturation profile, and marginally increased the total mass of methane in the coarse-grained layer (Table 4.3). Nonetheless, the measured differences are fairly insignificant in a 4 m-thick sand layer at rather low hydrate saturations.

Figure 4.7: $\alpha_{BSRZ} = 0.20\%$; $\lambda = 0.2 \cdot 10^{-13}$ s^{-1}; $D_m = 3.9 \cdot 10^{-10}$ m^2 s^{-1}

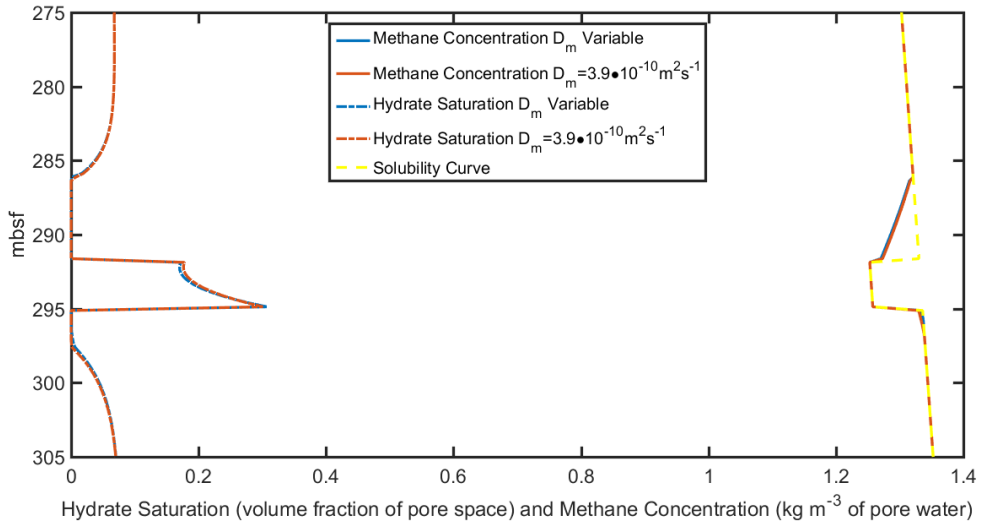

Table 4.3: D_m Analysis; * indicates values found in Hole H at Walker Ridge Block 313

α_{BSRZ} (%)	λ (s^{-1})	D_m (m^2 s^{-1})	HFZ above (m)	HFZ below (m)	h at upper boundary	h at lower boundary	min h in sand	mass CH_4 in sand (kg)
			10.3*	3.20*	.6*	.6*	.15*	
.10	$2.0 \cdot 10^{-13}$	Variable	3.00	1.00	.228	.347	.220	134.1
.10	$2.0 \cdot 10^{-13}$	$3.9 \cdot 10^{-10}$	3.00	1.25	.235	.342	.228	138.0
.20	$0.2 \cdot 10^{-13}$	Variable	5.75	1.00	.172	.307	.170	105.2
.20	$0.2 \cdot 10^{-13}$	$3.9 \cdot 10^{-10}$	5.75	2.25	.178	.301	.173	107.1

Additional Notes

Given the fairly small thickness of the sand layer modeled here, I investigated how a larger sand layer changes the hydrate saturation profile. Additionally, because the model behavior has a strong dependence on the concentration gradient between the two lithologies, I studied how a larger clay pore radius affected the findings. The simulated results can be found in Figures 4.8, 4.9, and 4.10.

Figure 4.8 Sand thickness = 3m, α_{BSRZ} = 0.10%; $\lambda = 0.5 \cdot 10^{-13}$ s^{-1}; D_m = variable, r_{sh} = 100nm.

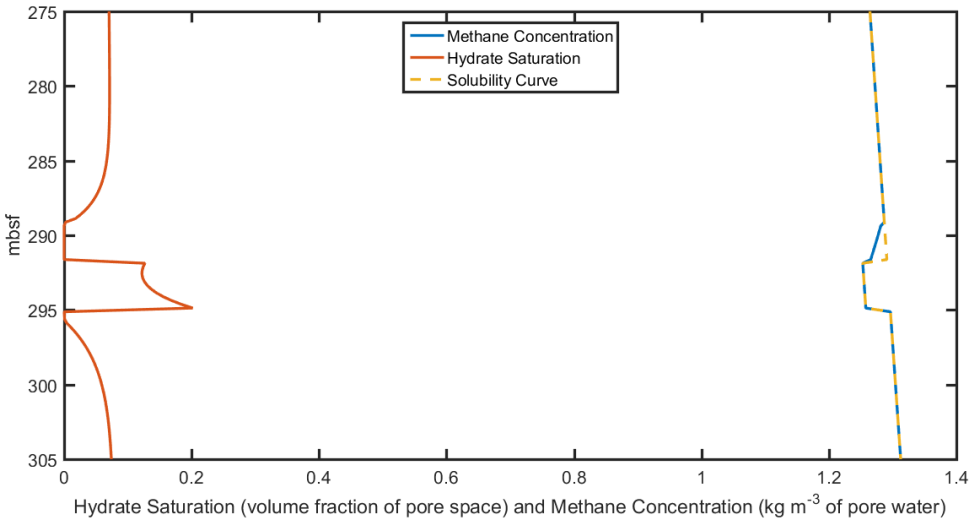

Figure 4.9 Increased sand thickness to 10m, α_{BSRZ} = 0.10%; $\lambda = 0.5 \cdot 10^{-13}$ s^{-1}; D_m = variable, r_{sh} = 100nm.

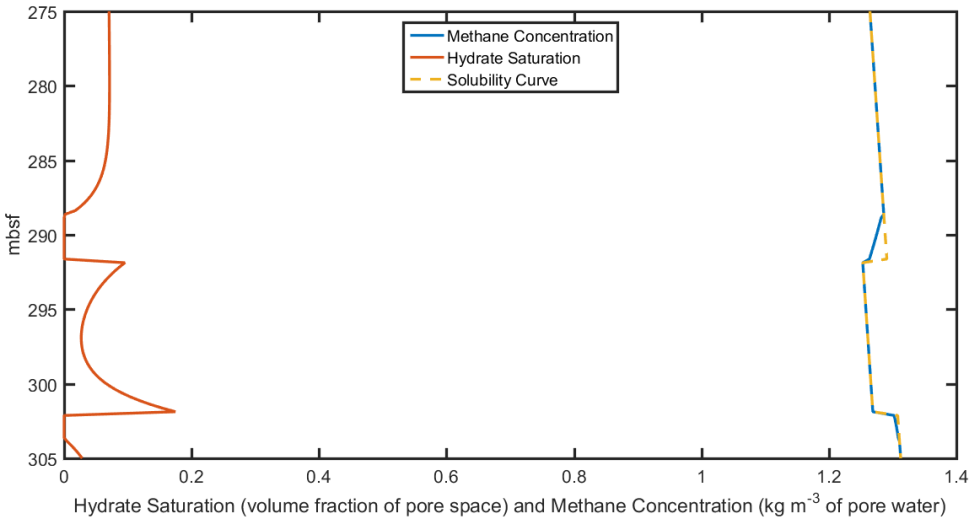

Figure 4.10: Increased sand thickness to 10m, $\alpha_{BSRZ} = 0.10\%$; $\lambda = 0.5 \cdot 10^{-13}$ s^{-1}; D_m = variable, $r_{sh} = 50$nm.

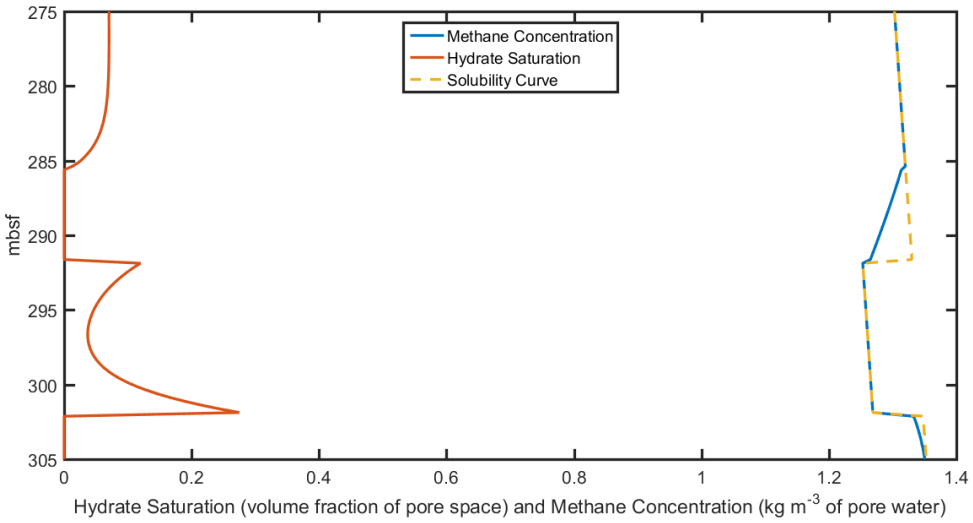

As shown, both the thickness of the sand and the assumed clay radius had a large effect on the hydrate saturation profile in the coarse-grained bed and its surroundings (Table 4.4). With a sand thickness of 10m and the only difference being the radius of the clay particles, the lengths of the HFZs above and below the sand were reduced by 50% and 43% respectively, the saturations at the upper and lower sand boundaries decreased by 21% and 36% respectively, and the total mass of methane declined by 35%. Similar results were produced while holding the sand thickness constant at 3m.

The increased thickness of the sand caused an increase in magnitude in both of the hydrate-free zones above and below the sand, smaller hydrate saturations at the sand boundaries, and a slight increase in total mass of methane. Holding the clay radius constant at 100nm, the HFZ above and below the sand was increased by 0.50 meters and 2.00 meters respectively, the saturations at the upper and lower sand boundaries decreased by 25% and 13% respectively, and the total mass of methane increased by 21%. Interestingly, doubling

the clay pore size had a far more significant effect on the hydrate saturation behavior compared to more than tripling the thickness of the sand layer.

Table 4.4: Additional analysis that includes the thickness of the sandstone bed and the assumed clay pore radius

r_{sh} (nm)	Sand thickness (m)	HFZ above (m)	HFZ below (m)	*h* at upper boundary	*h* at lower boundary	min *h* in sand	mass CH_4 in sand (kg)
50	3	5.75	1.75	.174	.310	.172	106.7
50	10	6.50	3.50	.120	.275	.037	121.1
100	3	2.75	0.00	.127	.202	.122	65.51
100	10	3.25	2.00	.095	.175	.027	79.11

4.2 DISCUSSION

The Impact of Key Parameters on Hydrate Saturation

In general, the hydrate formation behavior in coarse-grained layers was modeled as expected. The concentration gradient between the clay and sand lithologies caused the methane dissolved in pore water to diffuse into the coarse-grained layer. Additionally, evidence of two distinct features of hydrate formation in sand were seen in the above simulations. The first feature is the hydrate free zones bordering the sand layer, and the second is the rind that forms due to the dissolved methane forming hydrate immediately upon entering the coarse-grained sediment. However, the different parameters studied did not always affect the hydration saturation profile as anticipated.

As discussed, changing the amount of metabolizable organic carbon and rate constant of methanogenesis produced similar trends in the coarse-grained hydrate saturation profile, albeit by slightly different processes. Increasing λ causes methane to be generated faster, resulting in an increase of methane available for hydrate formation at shallower depths. In contrast, larger values of α_{BSRZ} increases the amount of methane

available for hydrate at all depths. The general increase in available methane caused the hydrate-free zones to diminish and the saturations in both the clay and sand to increase, but not to the magnitude anticipated. It is possible that the increased hydrate saturation observed in the clays actually restricted the movement of the dissolved methane and limited the increase in hydrate saturation within the sand. Also, it is not immediately clear why changing the rate constant of methanogenesis produced a more distinct rind in the sand layer.

While changing the diffusion coefficient of methane produced the desired result, the effect was not very substantial. A constant diffusion coefficient overestimated the amount of methane present as well as produced a slightly more homogenous hydrate saturation profile. This is due to a slight preservation of the flow pathways into and within the sand bed. Again, the observed effect was not very significant possible due to the fact that a decreasing porosity as a function of hydrate saturation minimizes the methane transport enough on its own.

Increasing both the thickness of the sand layer and the radius of the clay particles was shown to have a pronounced influence on the hydrate saturation profile. When the sand thickness is increased the hydrate rind is much more pronounced, and this result is likely due to the fact that there is very little concentration gradient within the sand itself. The lack of gradient does not encourage the migration of methane into the center of the sand, and this behavior is exhibited more clearly in a larger sand body. Therefore, in order to create massive hydrate deposits in thick sand layers, an upward fluid flux is likely needed. In addition, the increased volume of sand does provide more pore space for hydrate formation which explains the larger hydrate free zones and increase in mass of methane. However, increasing the clay pore radius created a marked decrease in absolute hydrate saturation and total mass of methane which emphasizes the importance of the

concentration gradient between lithologies and solidifies pore size as a key driver of hydrate growth.

Comparison to Walker Ridge

As shown in the results portion of this chapter, there was not a satisfactory match between simulated hydrate saturations in sand and the hydrate saturations observed in Walker Ridge Block 313 Hole H. Parameters that led to an increase in hydrate saturation inevitably led to a decrease in thickness of the HFZs, and limiting the formation of hydrate in the clays restricted the maximum hydrate saturations in the sand layer. The hydrate saturations at the boundaries of the sand never approached those seen in Hole H. I believe this result was largely due to the homogenous nature of the developed model.

Figure 4.11: Theoretical methane hydrate growth with the addition of highly permeable sands

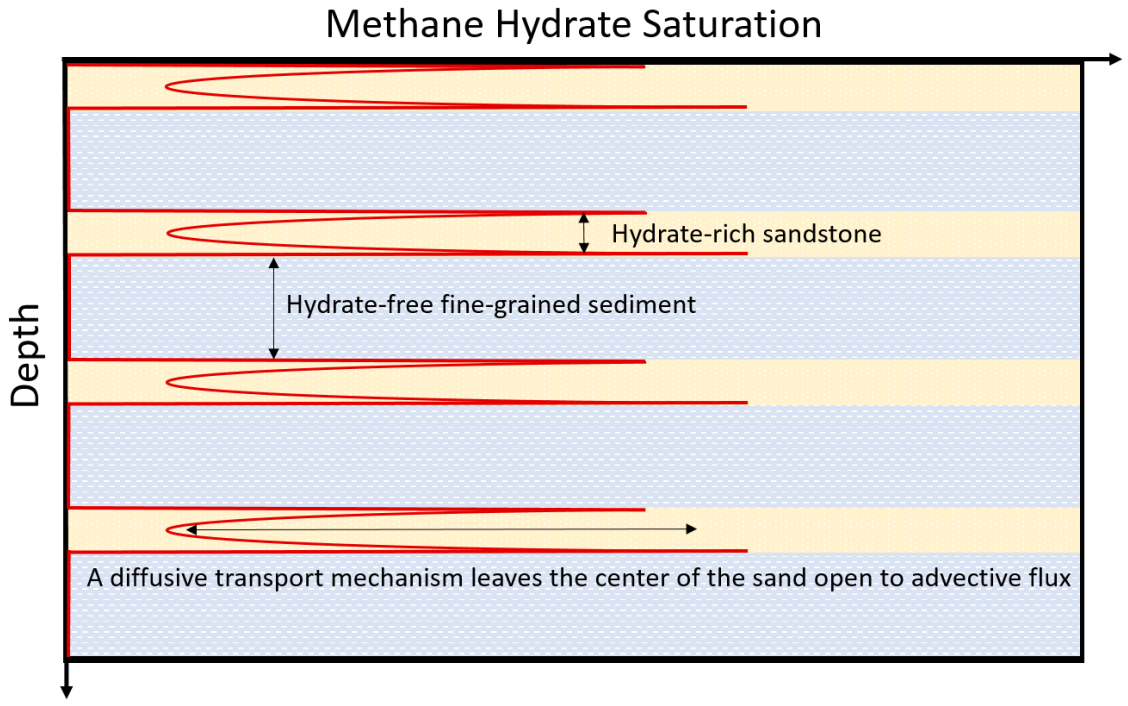

The log data obtained from Hole H showed significant fracturing within the clay layers as well as multiple layers of sand throughout the sediment column. Boswell et al. (2011) stated that sand lithology may comprise as much as 20% of the shallow sedimentary basin. Both of these features would draw dissolved methane out of the fine-grained sediment matrix thereby keeping the hydrate saturation low. Keeping the saturation low could preserve the fluid transport pathways between the clay and the sand. The scenario imagined here would allow a significantly higher weight percentage of available metabolizable organic carbon to produce the relatively high hydrate saturations seen in the log measurements while at the same time keeping the hydrate saturations low in the clay matrix (Figure 4.11).

Chapter 5: Conclusion

5.1 Conclusions

- A one dimensional model of hydrate growth was successively implemented, and the simulations helped to solidify the proposed models of hydrate formation in sand lithology with diffusion as the primary methane transport mechanism.
- Both increasing the amount of metabolizable organic carbon and the rate at which it is transformed into dissolved methane increased the amount of saturation in the fine and coarse-grained sediment.
- Changing the diffusion coefficient of methane as a function of hydrate saturation does not play a significant role in producing the expected hydrate saturation profile in a sand body.
- Diffusion acting as the only methane transport mechanism severely limits the possibility of thick accumulations of hydrate, especially in thicker sand layers.
- Larger sand beds are more efficient at preserving a permeable pathway in the middle of the coarse-grained layer. As a result, thicker beds are not conducive towards the formation of thick hydrate deposits with diffusion acting as the only methane transport mechanism.
- Heterogeneity likely plays a significant role at Walker Ridge Block 313 in keeping hydrate saturations low in fine grained sediment while providing enough methane to create hydrate saturations as large as .60 at the sand boundaries.

5.2 Future Recommendations

The model developed here was fairly homogenous and exceedingly simple compared to the complex nature of proper hydrogeologic systems. Moving forward, I would like to add a series of complexities in order to run more sophisticated simulations. The next logical step in creating simulations that are more applicable to actual shallow oceanic basins is to introduce an advective flow term into the already developed model in order to see its effect on the distribution of methane hydrate in a sandstone matrix. Currently, the pore fluid is stationary in the sediment column and only moves if there is a concentration gradient due to varying pore sizes. This phenomenon became most evident in the 10 m-thick sandstone layers. It would be interesting to see if the addition of a supplementary flow term would create a more homogenous hydrate saturation profile in coarse-rained beds. Further, the introduction of a Neumann boundary condition at a grid block marking the base of the gas hydrate stability zone would induce an upward flux as well as an additional source of methane.

In addition, due to the fact that conditions at Walker Ridge Block 313 were not recreated, it would be highly beneficial to include more high permeability features to test the idea that the heterogeneous sediment plays a key role in the observe hydrate saturation profile. This proposal would include a higher percentage of sand beds in addition to fractures within the fine-grained matrix. The addition of highly permeable fracture planes would involve updating the model to two, and eventually three, dimensions. Ideally, the work completed here is merely the foundation of a true basin-scale model for methane hydrate formation in continental margin sediments.

References

Archer, D. (2007). Methane hydrate stability and anthropogenic climate change. *Biogeosciences Discussions*, *4*(2), 993-1057.

Archer, D., Buffett, B., & Brovkin, V. (2009). Ocean methane hydrates as a slow tipping point in the global carbon cycle. *Proceedings of the National Academy of Sciences*, *106*(49), 20596-20601.

Archie, G. E. (1942). The electrical resistivity log as an aid in determining some reservoir characteristics. *Transactions of the AIME*, *146*(01), 54-62.

Berner, R. A. (1980). *Early diagenesis: A theoretical approach* (No. 1). Princeton University Press.

Boswell, R., & Collett, T. S. (2011). Current perspectives on gas hydrate resources. *Energy & environmental science*, *4*(4), 1206-1215.

Boswell, R., Collett, T. S., Frye, M., Shedd, W., McConnell, D. R., & Shelander, D. (2012). Subsurface gas hydrates in the northern Gulf of Mexico. *Marine and Petroleum Geology*, *34*(1), 4-30. (bghsz and maybe a couple other WRid stuff)

Buffett, B. A. (2000). Clathrate hydrates. *Annual Review of Earth and Planetary Sciences*, *28*(1), 477-507.

Claypool, G. E., & Kaplan, I. R. (1974). The origin and distribution of methane in marine sediments. In *Natural gases in marine sediments* (pp. 99-139). Springer US.

Clennell, M. B., Hovland, M., Booth, J. S., Henry, P., & Winters, W. J. (1999). Formation of natural gas hydrates in marine sediments: 1. Conceptual model of gas hydrate growth conditioned by host sediment properties. *Journal of Geophysical Research: Solid Earth*, *104*(B10), 22985-23003.

Cook, A. E., & Malinverno, A. (2013). Short migration of methane into a gas hydrate-bearing sand layer at Walker Ridge, Gulf of Mexico. *Geochemistry, Geophysics, Geosystems*, *14*(2), 283-291.

Daigle, H., & Dugan, B. (2011). Capillary controls on methane hydrate distribution and fracturing in advective systems. *Geochemistry, Geophysics, Geosystems*, *12*(1).

Davie, M. K., & Buffett, B. A. (2001). A numerical model for the formation of gas hydrate below the seafloor. *Journal of Geophysical Research: Solid Earth*, *106*(B1), 497-514.

Davie, M. K., & Buffett, B. A. (2003). A steady state model for marine hydrate formation: Constraints on methane supply from pore water sulfate profiles. *Journal of Geophysical Research: Solid Earth*, *108*(B10).

Davie, M. K., Zatsepina, O. Y., & Buffett, B. A. (2004). Methane solubility in marine hydrate environments. *Marine geology*, *203*(1), 177-184.

Dickens, G. R., O'Neil, J. R., Rea, D. K., & Owen, R. M. (1995). Dissociation of oceanic methane hydrate as a cause of the carbon isotope excursion at the end of the Paleocene. *Paleoceanography*, *10*(6), 965-971.

Everett, D. H. (1961). The thermodynamics of frost damage to porous solids. *Transactions of the Faraday society*, *57*, 1541-1551.

Harvey, L. D., & Huang, Z. (1995). Evaluation of the potential impact of methane clathrate destabilization on future global warming. *Journal of Geophysical Research: Atmospheres*, *100*(D2), 2905-2926.

Henry, P., Thomas, M., & Clennell, M. B. (1999). Formation of natural gas hydrates in marine sediments, 2, Thermodynamic calculations of stability conditions in porous sediments. *JOURNAL OF GEOPHYSICAL RESEARCH-ALL SERIES-*, *104*, 23-005.

Hyndman, R. D., & Davis, E. E. (1992). A mechanism for the formation of methane hydrate and seafloor bottom-simulating reflectors by vertical fluid expulsion. *Journal of Geophysical Research: Solid Earth*, *97*(B5), 7025-7041.

Kastner, M., Claypool, G., & Robertson, G. (2008). Geochemical constraints on the origin of the pore fluids and gas hydrate distribution at Atwater Valley and Keathley Canyon, northern Gulf of Mexico. *Marine and Petroleum Geology*, *25*(9), 860-872.

Klauda, J. B., & Sandler, S. I. (2005). Global distribution of methane hydrate in ocean sediment. *Energy & Fuels*, *19*(2), 459-470.

Kvenvolden, K. A. (1988). Methane hydrate—a major reservoir of carbon in the shallow geosphere?. *Chemical Geology*, *71*(1-3), 41-51.

Malinverno, A. (2010). Marine gas hydrates in thin sand layers that soak up microbial methane. *Earth and Planetary Science Letters*, *292*(3), 399-408.

Martens, C. S., & Berner, R. A. (1974). Methane production in the interstitial waters of sulfate-depleted marine sediments. *Science*, *185*(4157), 1167-1169.

Maslin, M., Owen, M., Betts, R., Day, S., Jones, T. D., & Ridgwell, A. (2010). Gas hydrates: past and future geohazard?. *Philosophical Transactions of the Royal Society of London A: Mathematical, Physical and Engineering Sciences*, *368*(1919), 2369-2393.

Milkov, A. V., & Sassen, R. (2001). Estimate of gas hydrate resource, northwestern Gulf of Mexico continental slope. *Marine Geology*, *179*(1), 71-83.

Milkov, A. V. (2004). Global estimates of hydrate-bound gas in marine sediments: how much is really out there?. *Earth-Science Reviews*, *66*(3), 183-197.

Paull, C. K., Matsumoto, R., Wallace, P., & And 25 others. (1996). Proceedings of the Ocean Drilling Program, Vol. 164, Initial Reports, Gas Hydrate Sampling on the Blake Ridge and Carolina Rise. Ocean Drilling Program.

Peters, E. J. (2012). *Advanced Petrophysics* (Vol. 2). Greenleaf Book Group.

Reeburgh, W. S. (2007). Oceanic methane biogeochemistry. *Chemical Reviews*, *107*(2), 486-513.

Rempel, A. W., & Buffett, B. A. (1997). Formation and accumulation of gas hydrate in porous media. *Journal of Geophysical Research: Solid Earth*, *102*(B5), 10151-10164.

Rempel, A. W. (2011). A model for the diffusive growth of hydrate saturation anomalies in layered sediments. *Journal of Geophysical Research: Solid Earth*, *116*(B10).

Sloan Jr, E. D., & Koh, C. (2007). *Clathrate hydrates of natural gases*. CRC press.

Stoll, R. D., Ewing, J., & Bryan, G. M. (1971). Anomalous wave velocities in sediments containing gas hydrates. *Journal of Geophysical Research*, *76*(8), 2090-2094.

Tréhu, A. M., Ruppel, C., Holland, M., Dickens, G.R., Torres, M.E., Collett, T.S., Goldberg, D.S., Riedel, M., Schultheiss, P. (2006). Gas hydrates in marine sediments:nLessons from scientific ocean drilling, Oceanography, 19, 124–142.

Ullman, W. J., & Aller, R. C. (1982). Diffusion coefficients in nearshore marine sediments. *Limnology and Oceanography*, *27*(3), 552-556.

Westbrook, G. K., Carson, B., Musgrave, R. J., and Leg 146 Scientific Party. (1994). Proceedings of the Ocean Drilling Program, Vol. 146, Initial Reports. Ocean Drilling Program

Zatsepina, O. Y., & Buffett, B. A. (1998). Thermodynamic conditions for the stability of gas hydrate in the seafloor. *Journal of Geophysical Research: Solid Earth*, *103*(B10), 24127-24139.